

Highly Selective Drug-Derived Fluorescent Probes for the Cannabinoid Receptor Type 1 (CB₁R)

AUTHOR NAMES

Leonard Mach,^[a] Anahid Omran,^[a] Jara Bouma,^[b] Silke Radetzki,^[a] David A. Sykes,^[c,d] Wolfgang Guba,^[e] Xiaoting Li,^[f,g] Calvin Höffelmeyer,^[a] Axel Hentsch,^[a] Thais Gazzini,^[a] Yelena Mostinski,^[a] Malgorzata Wasinska-Kalwa,^[a] Fabio de Molnier,^[h] Cas van der Horst,^[b] Jens Peter von Kries,^[a] Marc Vendrell,^[h] Tian Hua,^[f,g] Dmitry B. Veprintsev,^[c,d] Laura H. Heitman,^[b] Uwe Grether,^[e] Marc Nazare^[a]**

AUTHOR ADDRESS

^[a] Leibniz-Forschungsinstitut für Molekulare Pharmakologie (FMP), 13125 Berlin (Germany)

^[b] Division of Drug Discovery and Safety, Leiden Academic Centre for Drug Research, Leiden University, and Oncode Institute, 2333 CC, Leiden (The Netherlands)

^[c] Division of Physiology, Pharmacology & Neuroscience, School of Life Sciences, University of Nottingham, Nottingham, NG7 2UH (United Kingdom)

^[d] Centre of Membrane Proteins and Receptors (COMPARE), University of Birmingham and University of Nottingham, Midlands (United Kingdom)

^[e] Roche Pharma Research & Early Development, Roche Innovation Center Basel, F. Hoffmann-La Roche Ltd., 4070 Basel (Switzerland)

^[f] iHuman Institute, ShanghaiTech University, Shanghai 201210 (China)

^[g] School of Life Science and Technology, ShanghaiTech University, Shanghai 201210 (China)

^[h] IRR Chemistry Hub and Centre for Inflammation Research, Institute for Regeneration and Repair, University of Edinburgh, EH16 4UU (United Kingdom)

KEYWORDS

Fluorescent probes, Cannabinoid receptor type 1, Imaging, TR-FRET

ABSTRACT

The cannabinoid receptor type 1 (CB₁R) is one of the central elements of the endocannabinoid system regulating a variety of signaling cascades. Extensive efforts on CB₁R have validated its essential roles in physiology such as appetite regulation, pain perception, memory formation, and thermoregulation. Yet, there is a surprising lack of clear understanding of its cellular signaling, distribution, and expression dynamics. CB₁R visualization in real-time is therefore crucial for addressing these open questions in cannabinoid research. Using various highly selective drug-like CB₁R ligands with a defined pharmacological profile, we investigated their potential for constructing CB₁R fluorescent probes by a reverse design-approach. A modular design concept with a diethyl glycine-based building block as centerpiece allowed the straightforward modular

synthesis of novel probe candidates. Supported by computational docking studies, this systematic approach led to the identification of novel pyrrole-based CB₁R fluorescent probes. The probes demonstrated CB₁R selectivity in radioligand binding profiling and inverse agonist activity in a cAMP assay. Application in time-resolved fluorescence resonance target-engagement studies and CB₁R live cell imaging exemplify the great versatility of the tailored pyrrole-based fluorescent probes. These validated fluorescent probes aim to deepen the understanding of mechanistic aspects of CB₁R localization, trafficking, and activation essential for the function and role of this receptor in pathological conditions.

INTRODUCTION

Present in all vertebrates, the cannabinoid receptor type 1 (CB₁R), alongside the cannabinoid receptor type 2 (CB₂R), is the key signal transducer of the endocannabinoid system (ECS).¹ CB₁R is predominantly expressed on presynaptic terminals in the central nervous system (CNS) where it modulates neuronal signaling.^{2,3} Yet, CB₁R was also found on peripheral cells and organs.^{4,5} In conjunction with its localization, CB₁R has implications in the homeostasis of various fundamental physiological processes, such as appetite regulation,⁶ energy metabolism,⁷ synaptic plasticity,⁸ and nociception⁹. Most relevant, aberrant expression of CB₁R is associated with pathophysiological processes among them neurodegenerative diseases, neurological, metabolic and inflammatory disorders.^{10,11} This plethora of potential therapeutic indications underlines the clinical relevance and has triggered extensive pharmaceutical research on CB₁R.^{12,13} However, the withdrawal of the inverse agonist Rimonabant (**6**, Figure 2) as an anti-obesity agent from the European market in 2008 represented a major incision in CB₁R drug research.^{14,15} The complexity of ECS signaling and the CB₁R-related CNS side effects have called for appropriate analytical tools to advance a deeper understanding of the involvement of the CB₁R in the ECS.¹⁶ For translation of novel promising CB₁R drug candidates¹⁷⁻²⁴ emerging from pre-clinical studies to clinical trials visualization tools for spatio-temporally resolved CB₁R pharmacological characterization are urgently required.²⁵

Fluorescence-based techniques have evolved into a powerful method for studying G-protein coupled receptors (GPCRs).^{26,27} In particular, small molecule fluorescent probes represent versatile tools to elucidate various mechanistic aspects of GPCR pharmacology. Among them are the detection of time-resolved target engagement, allosterism, internalization, dimerization, or membrane organization at cellular level.²⁸⁻³³ While several CB₂R fluorescent probes were recently

reported, only a few CB₁R fluorescent probes have been described so far.^{34,35} The only two examples of CB₁R imaging probes are phytocannabinoid-derived (**1** and **2**, Figure 1).^{36, 37} In general, issues associated with phytocannabinoid probes are their limited selectivity over CB₂R and lipophilicity that may result in high unspecific background signal. Besides phytocannabinoids, synthetic drug-derived fluorescent probes have been reported (e.g. **3**). However, their selective CB₁R application was not validated further.^{30, 38, 39} In turn, no CB₁R-selective imaging probe is described that has been unambiguously characterized pharmacologically in terms of its functional activity and selectivity profile. However, knowledge of the detailed mechanism of action of an imaging probe is crucial to obtain definite and relevant biological results on live cells, as the probe represents a pharmacological active unit itself. For example, GPCR agonists may induce receptor internalization relevant for internalization studies, whereas an inverse agonist may allow the detection of steady-state membrane receptor pools.⁴⁰

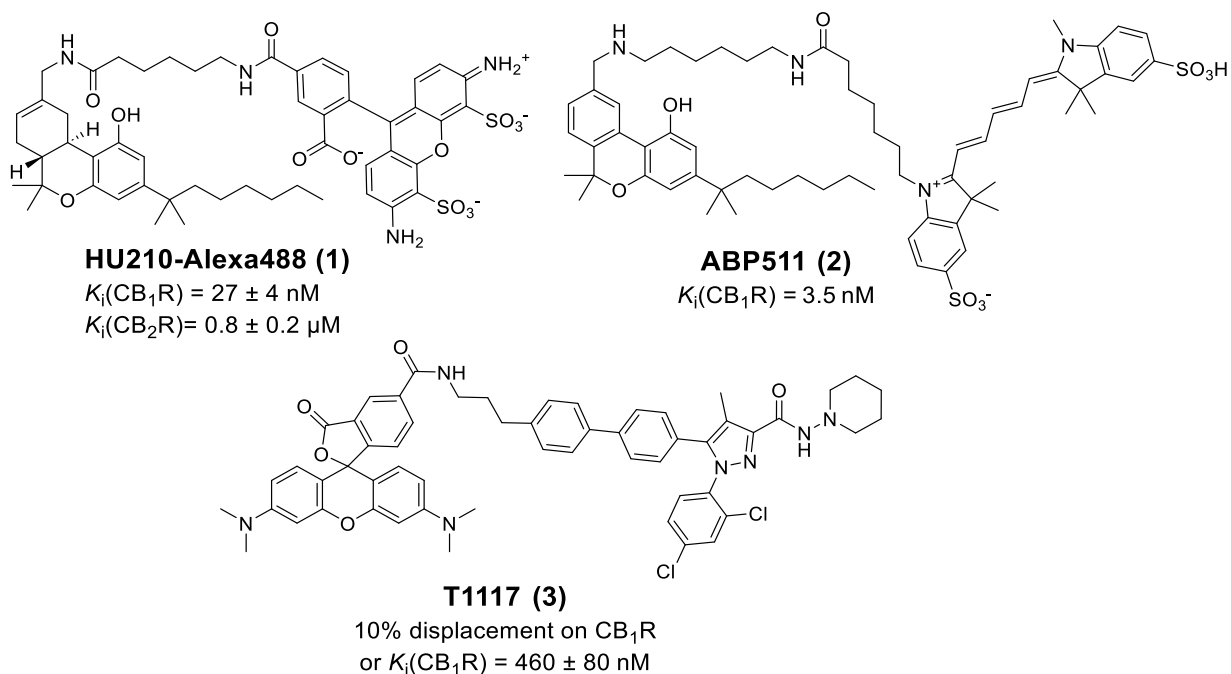


Figure 1. Structures of selected small molecule CB₁R fluorescent probes.^{30, 36, 37, 39}

Herein, we report the modular design, synthesis, pharmacological evaluation, and application of CB₁R-selective fluorescent probes. The probes were conceptualized based on a reverse design approach employing synthetic drug-like CB₁R ligands with a defined pharmacological profile as starting points.⁴¹ This study led to the discovery of novel and highly selective pyrrole-based CB₁R fluorescent probes. Further exploration showcased the versatility of these inverse agonist fluorescent probes for pharmacological time-resolved Förster resonance transfer (TR-FRET) studies and CB₁R imaging on live cells. Our approach presents a viable design concept for future CBR probes leveraging a deeper understanding of CB₁R pharmacology.

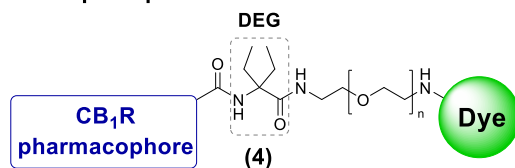
DESIGN CONCEPT

Previously, we reported a series of CB₂R-selective fluorescent probes derived from CB₂R ligands bearing an α , α -diethyl glycine (DEG) moiety as a versatile and suitable centerpiece for linker attachment.⁴² As an amino acid, the DEG motif has granted a high flexibility and synthetic simplicity for amide bond-based derivatization by different pharmacophoric units and linkers achieving CB₂R probes. Here, we aimed to expand the design scope of this privileged and chemically stable DEG-based probe design toward a CB₁R probe platform (**4**, Figure 2A). Attempting this, candidate structures as pharmacophore donors were selected among six high-affinity drug-like CB₁R ligands (**5-10**, Figure 2B). Requirements for selection were a central amide bond to facilitate the attachment to the DEG centerpiece, structural diversity, and varied functionalities e.g. inverse agonist, antagonist, and agonist.⁴³⁻⁴⁶

The probe design was based on three exploration steps to achieve validation of our construction concept. We first replaced the original apolar amine unit in **5-10** with DEG ethyl ester to examine

whether this modification would be tolerated (Figure 2C). Ideally, the original pharmacological properties of the parent compounds, such as high affinity, functional activity, and selectivity for CB₁R, would be preserved upon these structural changes. In a second and third step, the influence of linker attachment and then of fluorophore installation was investigated, respectively (Figure 2C). Structure-activity relationship (SAR) was screened throughout the series with pharmacological characterization of binding affinity to CB₁R and CB₂R.

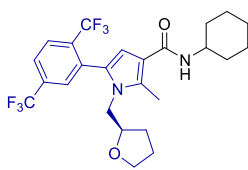
A) General construction principle:



CB₁R Building block scheme

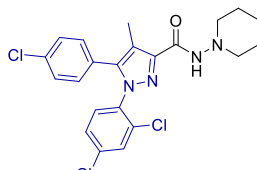
DEG: α,α -diethyl glycine

B) CB₁R ligands screened:



(5)

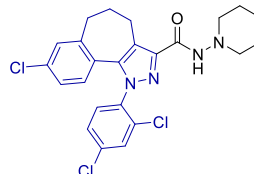
$IC_{50}(CB_1R) = 8$ nM
 $IC_{50}(CB_2R) > 80$ nM
 inverse agonist



(6)

Rimonabant

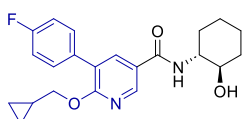
$K_i(CB_1R) = 8$ nM
 $K_i(CB_2R) = 790$ nM
 inverse agonist



(7)

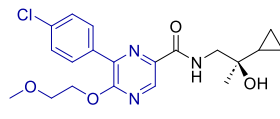
NESS-0327

$K_i(CB_1R) = 4.2$ nM
 $K_i(CB_2R) = 55.7$ nM
 neutral antagonist



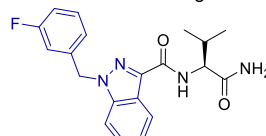
(8)

$K_i(CB_1R) = 42.8$ nM
 $K_i(CB_2R) > 10000$ nM
 inverse agonist



(9)

$K_i(CB_1R) = 47.5$ nM
 $K_i(CB_2R) > 475$ nM
 inverse agonist



(10)

AB-FUBINACA 3-F benzyl

$K_i(CB_1R) = 12.6$ nM
 $K_i(CB_2R) = 52.5$ nM
 agonist

C) Example of the modular CB₁R probe design concept:

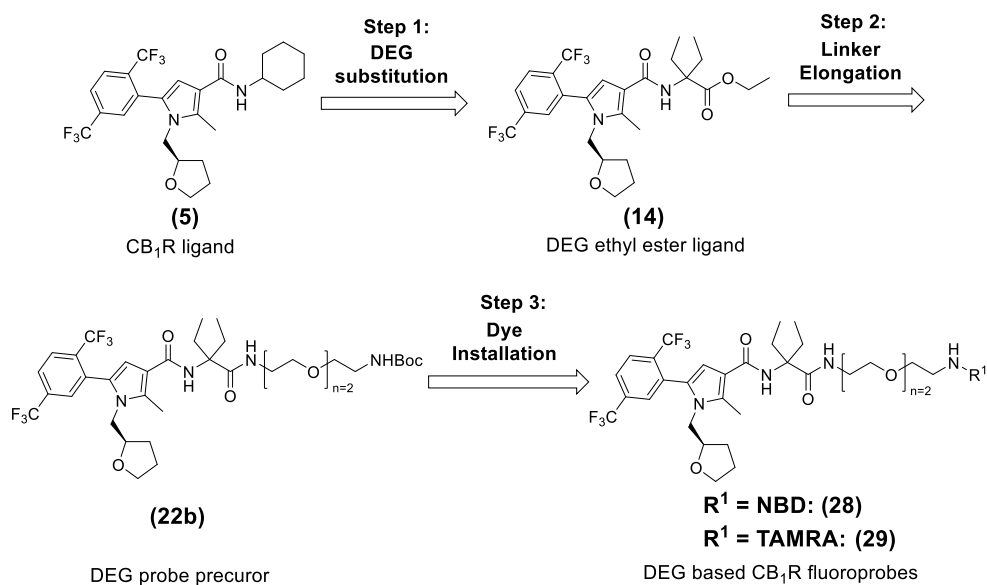


Figure 2: α , α -Diethyl glycine (DEG) amide probe design approach. A) General construction scheme for CB₁R fluorescent probes based on DEG. B) Selected drug-like CB₁R ligands⁴³⁻⁴⁸ bearing amide bonds are useful as donors for CB₁R pharmacophoric units (blue) for the attachment to the DEG centerpiece. Amine fragments (black) were replaced with DEG. C) Exemplified three-step probe exploration for CB₁R pyrrole-based fluorescent probes **28** and **29**.

RESULTS AND DISCUSSION

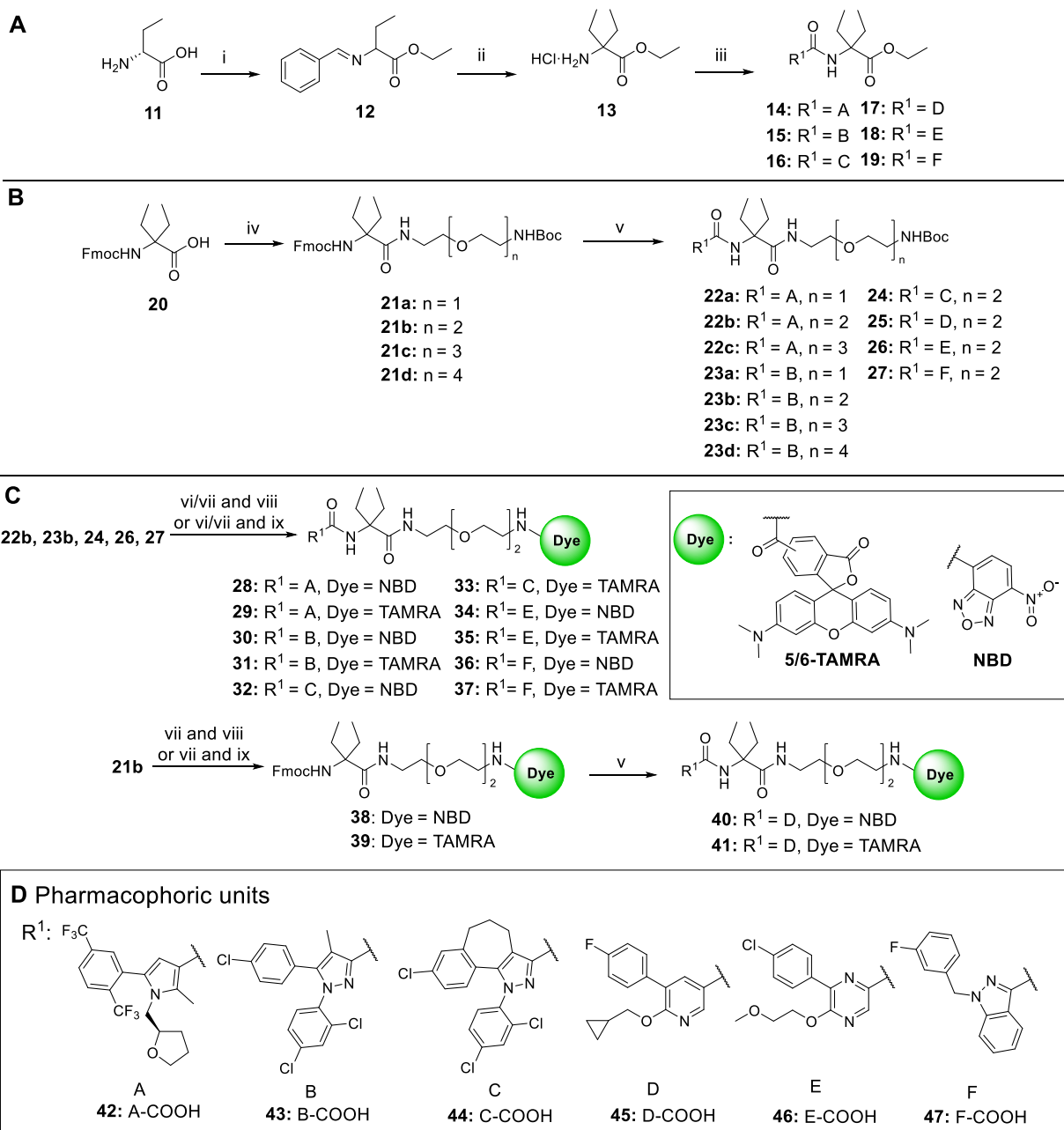
Chemistry

The synthesis of the parent DEG ethyl ester compounds **14-19** is outlined in Scheme 1A. The synthesis began with SOCl₂-facilitated esterification of the carboxylic acid functional group of **11** followed by benzyl protection of the amino group to give benzylidene intermediate **12**. The central DEG building block **13** was obtained via an alkylation of **12** using ethyl iodide and KHDMS followed by hydrolysis of the benzylimine under acidic conditions. HATU-mediated amide coupling reaction with respective carboxylic acids **42-47** furnished the desired DEG ligands **14-19**.

To determine the optimal linker length for the dye attachment, commercially available *N*-Fmoc- α , α -diethyl glycine **20** was utilized (Scheme 1B). Using an orthogonal protecting group strategy, a series of *N*-Boc protected diamine linkers (n=0-4) were coupled to amino acid **20** using HATU to give access to **21a-d**. Fmoc-protecting group removal of compounds **21a-d** using DBU was followed by *in situ* coupling to corresponding carboxylic acids **42-47** to afford Boc-protected congeners **22a-c**, **23a-d**, and **24-27**. Notably, the HATU coupling of **42** with Fmoc-deprotected **22a-c** resulted in consistently low yields with an unreactive HOAt-ester intermediate as the main

product (**S53**, see Supporting Information Figure S21). This observation could be attributed to the steric hindrance of DEG which is known to be a challenging factor in amide couplings.⁴⁹ The initially observed low yields of <10% yield for the amide coupling reaction (see **22a**) were improved for **22b** and **22c** by increasing the temperature to 40 °C - 45 °C and prolongation of the reaction times to 4-7 days (56% and 48% yield, respectively).

Scheme 1. General synthetic routes for the construction of evaluated ligands^a



^aA) Synthesis of the parent DEG ethyl ester compounds **14-19**: Reagents and conditions: i) a) SOCl₂, EtOH, 0 °C to reflux; 5 h; b) benzaldehyde, TEA, DCM, MgSO₄, rt, 30 h; ii) a) KHDMS, EtI, THF, -70 °C to rt, 24 h; b) HCl, Et₂O, 0 °C to rt, 15 h; iii) **42-47**, HATU, DIPEA, DMF, 3 h, rt. B) Synthesis of linker library **22a-27**. Reagents and conditions: iv) HATU, BocNH-CH₂CH₂(OCH₂CH₂)_n-NH₂ (n=1-4), DIPEA, DMF, 3 h, rt; v) DBU, DMF, then HOAt, then **42-47**, HATU, DIPEA, DMF, 3 h-6 d, rt-45 °C. C) Synthesis of fluorescent probes **28-37**: Reagents and conditions: For **28** and **29** vi) HFIP, MW, 90 min, 150 °C. For **30**, **32**, **34**, **36** vii) TFA, DCM, 2 h, rt. then viii) NBD-F, DIPEA, DMF, 18 h. ix) TAMRA-COOH, EDC·HCl, HOAt, DIPEA, DMF, 20 h, rt or TAMRA-SE, DIPEA, DMF, 2 h, rt. Synthesis of fluorescent probes **40-41**: Reagents and conditions: vii) TFA, DCM, 2 h, rt. viii) NBD-F, DIPEA, DMF, 18 h. ix) TAMRA-COOH, EDC·HCl, HOAt, DIPEA, DMF, 20 h, rt or TAMRA-SE, DIPEA, DMF, 2 h, rt. v) DBU, DMF,

then HOAt, then **45**, HATU, DIPEA, DMF, 3 h, rt. D) Pharmacophoric carboxylic acid units **42-47** derived from **5-10**.

To obtain target fluorescent probes **28-37** and **40-41**, the terminal *N*-Boc protecting group of **22b**, **23b**, and **24-27** had to be removed (Scheme 1C). Cleavage using TFA was applied for **23b**, **24**, **26** and **27**. This procedure, however, was not compatible with compounds **22b** and **25** where partial degradation in the presence of TFA was observed. To overcome this problem, Boc-deprotection of **22b** was performed under mild, microwave-assisted cleavage using 1,1,1,3,3,3-hexafluoroisopropanol (HFIP).⁵⁰ This procedure was found to be mild enough to avoid decomposition and yielded the free terminal amine of **22b**. The resulting free amines were coupled either to carboxy 5/6-tetramethyl rhodamine (TAMRA) fluorophore by amide coupling or to fluoro-nitrobenzoxadiazole (F-NBD) via nucleophilic aromatic substitution conditions to achieve probes **28-37** (see Supporting Information Figure S23-31). Boc-deprotection of **25** was neither possible with TFA nor under HFIP/MW conditions. Therefore, probes **40** and **41** were synthesized via a variation of the synthetic route starting with Boc-deprotection of **21b** followed by conjugation of fluorophores to obtain intermediates **38** and **39**. After the removal of the Fmoc-protecting group with DBU, another amide coupling under HATU conditions gave access to the fluorescent probes **40** and **41** (Scheme 1C, see Supporting Information Figure S32 und S33).

Computational Studies

Docking studies were conducted to explore the orientation of parent DEG esters **14-19**. Exemplified in Figure 3A is the docking structure of the DEG ethyl ester **14** derived from **5** in

inactive CB₁R (utilizing PDB ID: 5TGZ).⁵¹ Interestingly, the pharmacophoric pyrrole unit in **14** bearing the DEG centerpiece unit was well accommodated in the binding pocket of CB₁R aligning with the known co-crystallized ligand AM6538 (PDB ID: 5TGZ) (see Supporting Information Figure S12). The DEG unit in **14** was oriented toward the extracellular space comparable with the piperidine unit of AM6538. Docking poses of compounds **15-19** consistently showed that the ethyl ester moiety points toward the *N*-terminus of CB₁R (see Supporting Information, Figure S7-11). We therefore concluded that DEG can favorably replace the original amine units of **5-10** (Figure 2B, black fragments). Hence, utilization of the CB₁R pharmacophoric units from **5-10** in conjunction with a DEG centerpiece appeared as a promising approach toward a platform for CB₁R fluorescent probes. In addition, the docking study revealed that the terminal carboxy group of DEG is an ideal linker attachment site allowing free access to the extracellular space thereby avoiding extensive linker attachment studies (Figure 3A, B).

To estimate a proper linker length for dye attachment in our probes docking studies were performed on compounds **22b**, **23b**, **24-27** in the same receptor structure. The docking pose of **22b** is shown in Figure 3C (for compounds **23b**, **24-27** see Supporting Information Figure S7-11). The PEG chain with *n*=2 was predicted to reach out to the CB₁R extracellular site through the trans-membrane helices TM1 and 2. This linker appeared to be long enough to allow the envisioned fluorophore attachment at the terminal amine without interfering with binding (Figure 3D). A detailed SAR investigation on the linker length confirmed these results (see next section).

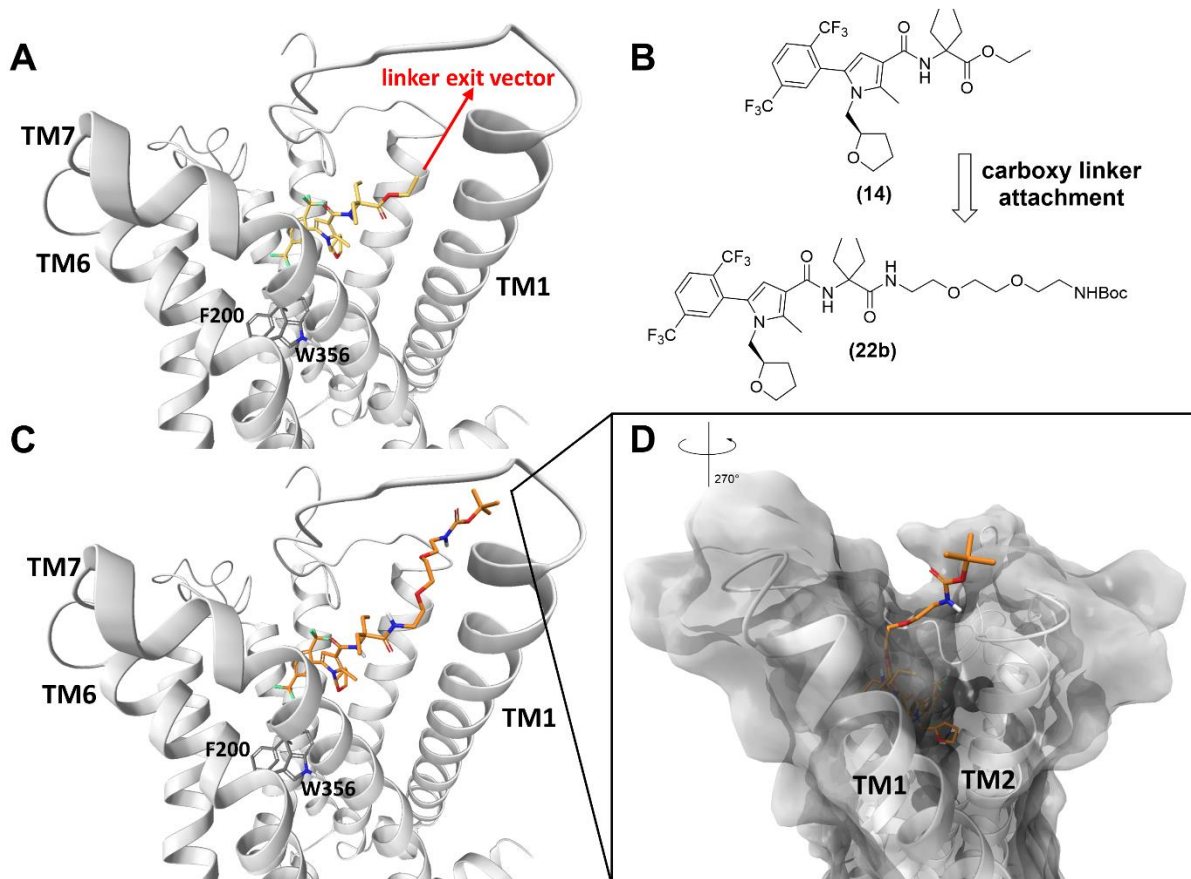


Figure 3. Docking poses of representative pyrrole-based CB₁R ligand **14** and DEG probe precursor **22b** in CB₁R inactive state (light grey, docked in PDB ID: 5TGZ, X-ray diffraction, 2.80 Å)⁵¹. A) Docking pose of parent DEG ethyl compound **14** (yellow) located in the binding pocket of CB₁R with ethyl ester group pointing towards the *N*-terminal site. B) Linker installation on **14** via the carboxy-terminal amide bond of DEG is a reasonable strategy based on the docking structures. C) DEG probe precursor **22b** with *n*=2 (orange). D) The linker reaches the CB₁R extracellular site through trans-membrane helices (TM) 1 and 2. For docking poses of **15-19**, **23b**, and **24-27** and a detailed description of the docking studies see Supporting Information.

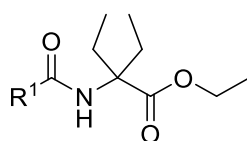
In Vitro Pharmacology

Pharmacological Profiling of DEG Ethyl Ester Intermediates

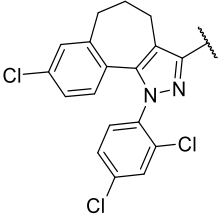
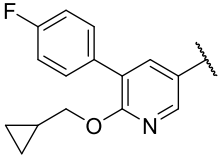
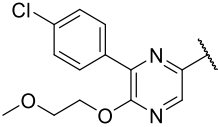
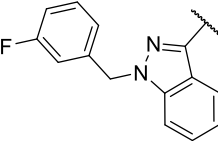
We first analyzed the novel drug-like DEG ester-derived CB₁R ligands **14-19** to experimentally examine whether the insertion of DEG moiety would be tolerated without compromising CB₁R affinity and functional activity compared to the parental counterparts **5-10** (Table 1). The binding affinities were measured in a radioligand binding assay on Chinese hamster ovary (CHO) membranes stably expressing either human CB₁R or CB₂R. In this assay, all compounds (**14-19**) exhibited nanomolar to sub-micromolar affinity for human CB₁R. However, among all tested chemotypes, only **14** preserved CB₁R affinity and showed pronounced selectivity for CB₁R ($K_i(\text{CB}_1\text{R}) = 11 \text{ nM}$; $K_i(\text{CB}_2\text{R}) = 306 \text{ nM}$, $K_i(\text{CB}_2\text{R})/K_i(\text{CB}_1\text{R}) = 28$ -fold selectivity). Notably, compounds **17** and **18** showed a swap from CB₁R-selectivity to CB₂R-selectivity. This finding could be attributed to the acquired structural similarity to 3,4,5-substituted pyridine CB₂R-ligands⁵² upon conjugation with the DEG ethyl ester. Even though the differences between the CB₁R and CB₂R binding affinities for compounds **15** and **16** were not pronounced, they exhibited a slight preference for CB₂R. Even though indazole-based **19** showed no CB₁R-selectivity after installation of the DEG moiety, the lack of CB₁R-selectivity was not surprising in this case as **19** was derived from agonist **10**, which already featured a weak CB₁R preference ($K_i(\text{CB}_2\text{R})/K_i(\text{CB}_1\text{R}) = 4$ -fold selectivity) commonly observed with this compound class.^{48, 53} In a CB₁R cAMP functional homogeneous time-resolved fluorescence (HTRF) assay⁵⁴ **14**, **15**, **17**, **18** were found to be inverse agonists and **19** an agonist, while **16** showed no activity in the assay. To our delight, all DEG esters retained the functional activity of their parent structures **5-10**.

Previous studies showed that linker and dye attachment can strongly affect the pharmacological profile of probes in an unpredictable fashion.⁵⁵⁻⁵⁷ Hence, to get an unbiased and detailed picture of the linker tolerance of the structures and optimal length for dye conjugation we progressed with a linker screen by using compound series **22a-c** and **23a-d** with *N*-Boc-protected terminus as parent model compounds.

Table 1. Binding affinities and functional activity of CB₁R DEG ligands



R ¹	Compound	Binding affinity		Functional activity
		hCB ₁ R <i>K_i</i> (nM) ^a	hCB ₂ R <i>K_i</i> (nM) ^a	(cAMP assay) EC ₅₀ or IC ₅₀ (nM) ^b (E _{max} (%)) ^c
	14	11	306	1.48 (-46)
	15	28	9	13.2 (-42)

	16	18	4	n.a.
	17	308	6	43.6 (-48)
	18	817	11	191 (-41)
	19	19	1	3.24 (93)

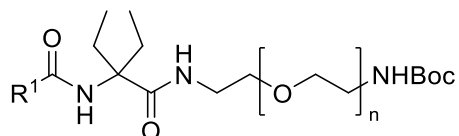
^a K_i (nM) values obtained from [³H]CP55,940 displacement assays on CHO membranes stably expressing human CB₁R or human CB₂R. Values are means of three independent experiments performed in duplicate. ^bThe activity levels (EC₅₀ or IC₅₀) of **14-19** were measured using cells stably expressing hCB₁R in homogeneous time-resolved fluorescence (HTRF) cAMP assay. The data are the means of three independent experiments performed in technical replicates. ^c Maximum effect (E_{max} in %) was normalized to reference full agonist CP55,940. n.a. denotes no activity.

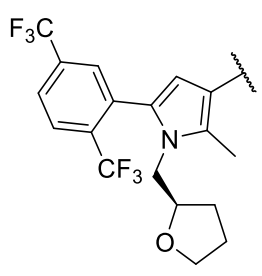
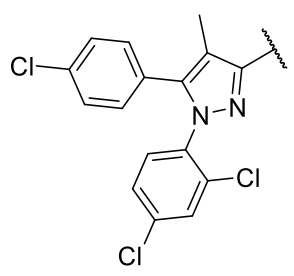
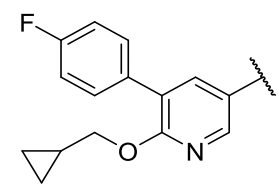
The pharmacological evaluation of the DEG probe precursors **22a-c**, **23a-d**, and **24--27** is outlined in Table 2. Even though the overall binding affinities of compounds **22a-c** declined compared to **14**, CB₁R preference was preserved. Despite the absence of a linear correlation between the linker length and binding affinities, linker length $n = 2$ of **22b** appeared as most favorable as it exhibited the highest CB₁R affinity and selectivity. In addition, **22b** retained inverse agonist activity (IC₅₀ = 131 nM, E_{max} = -69%). This linker selection was supported by our docking

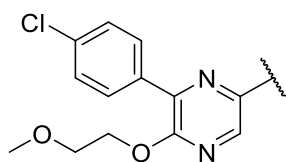
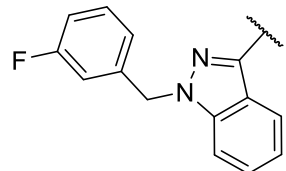
studies (Figure 3). We further examined the effect of the linker attachment and length on pyrazoles **23a-d** compared to parent **15**. Interestingly, while attachment of DEG ester in compound **15** attenuated its CB₁R-selectivity, installation of *N*-Boc-protected PEG chains in compounds **23a-d** revived the CB₁R-selectivity over CB₂R. Unlike **22a-c**, compounds **23a-d** showed a linear correlation between CB₁R affinity and the linker lengths. In this series **23a** (n=1) showed the highest affinity and selectivity to CB₁R. However, a short linker might lead to a steric clash with the receptor's binding pocket after the envisioned dye installation and consequently compromise binding affinity. Altogether, the molecular docking of **22b** and binding data of series **22a-c** and **23a-d** supported the selection of n=2 as the most suited linker for our probes. To our delight, **23b** also showed conserved functional activity as an inverse agonist on CB₁R (IC₅₀ = 64.6 nM, E_{max} = -44%).

The *N*-Boc-protected PEG chain with n=2, as the ideal linker, was also examined in combination with pharmacophores **44-47** yielding DEG probe precursors **24-27**. Unfortunately, compounds **24-27** exhibited no or significantly weaker CB₁R binding (between 3 μM and >10 μM) (Table 2) and instead CB₂R preference indicating that linker elongation is not equally well tolerated by all pharmacophores.

Table 2. Binding affinities and functional activity of the *N*-Boc-protected DEG probe precursors.



R ¹	Cmpd.	n	Binding affinity		Functional activity (cAMP assay)
			hCB ₁ R K _i (nM) ^a	hCB ₂ R K _i (nM) ^a	IC ₅₀ (nM) ^b (E _{max} (%) ^c)
	22a	1	1425	>10,000	n.d.
	22b	2	811	>10,000	131 (-69)
	22c	3	1219	>10,000	n.d.
	23a	1	37	1593	n.d.
	23b	2	139	>10,000	64.6 (-44)
	23c	3	397	2118	n.d.
	23d	4	603	2123	n.d.
	24	2	>10,000	776	n.d.
	25	2	3055	818	n.d.

	26	2	>10,000	701	n.d.
	27	2	>10,000	108	n.d.

^a K_i (nM) values obtained from [³H]CP55,940 displacement assays on CHO cell membranes stably expressing human CB₁R or human CB₂R. Values are means of three independent experiments performed in duplicate. ^bThe activity levels (IC₅₀) of **22b** and **23b** were measured using cells stably expressing hCB₁R in homogeneous time-resolved fluorescence (HTRF) cAMP assay. The data are the means of three independent experiments performed in technical replicates. ^cMaximum effect (E_{max} in %) was normalized to reference full agonist CP55,940. n.d. is not determined.

Pharmacological Profiling of CB₁R Fluorescent probes

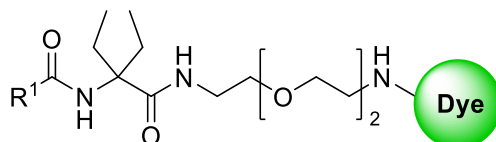
Next, we studied the CB₁R binding affinity of probes **28-37** and **40-41** equipped with fluorescent dyes NBD and TAMRA. As the presence of a fluorophore might significantly alter the pharmacological profile of the probes,^{55, 58, 59} we thoroughly characterized our target compounds (Table 3). In this study, we have chosen green-emitting NBD and orange-emitting TAMRA as examples for sterically small and large fluorophores, respectively. In addition, TAMRA as a partially zwitterionic hydrophilic rhodamine-derivative should be especially suited for cellular imaging of membrane proteins due to its good photostability and quantum yield. Photophysical characteristics of the probes were assessed in PBS buffer (Supporting Information Table S5). We determined the CB₁R and CB₂R binding profile of the labeled probes carrying different fluorophores in the radioligand binding assay and in the functional HTRF cAMP assay. We

observed fluorophore-dependent differences in the binding profile of the probes. For example, pyrrole-based probes **28** and **29** bearing NBD and TAMRA, respectively, maintained their CB₁R-selectivity. However, the substantially lower K_i value for TAMRA probe (**29**, $K_i(\text{hCB}_1\text{R}) = 2077$ nM, $K_i(\text{CB}_2\text{R})/K_i(\text{CB}_1\text{R}) > 4.8$) suggested that the larger TAMRA dye might interfere with ligand binding, while NBD conjugation turned out to be beneficial for the CB₁R affinity (**28**, $K_i(\text{hCB}_1\text{R}) = 97$ nM, $K_i(\text{CB}_2\text{R})/K_i(\text{CB}_1\text{R}) > 103$) when compared to the DEG probe precursor **22b** ($K_i(\text{hCB}_1\text{R}) = 811$ nM). In contrast to the binding assay, both inverse agonists **28** ($\text{IC}_{50} = 16.6$ nM) and **29** ($\text{IC}_{50} = 30.9$ nM) were more potent in the cAMP functional assay when compared to **22b** and with only weak dye-dependency. A similar effect was observed for pyrazole-based probes **30** and **31**. Inverse agonist NBD probe **30** ($K_i(\text{CB}_1\text{R}) = 428$ nM; $K_i(\text{CB}_2\text{R})/K_i(\text{CB}_1\text{R}) > 23$, $\text{IC}_{50} = 60.1$ nM) preserved its CB₁R profile when compared to precursor **23b** while TAMRA conjugation was deleterious for the binding affinity of **40** to either of the CBRs. To our surprise, the indazole-based NBD probe **36** showed binding to CB₁R ($K_i(\text{CB}_1\text{R}) = 1174$ nM) while its DEG probe precursor **27** and TAMRA congener **37** were solely CB₂R binders. Yet, both showed preferred binding to CB₂R. Similarly, rigidified pyrazole **32**, pyridine **40** and pyrazine **34** NBD probes displayed CB₂R selectivity. Within this series, dye-dependency was observed again, as with their respective TAMRA congeners **33**, **41**, and **35** did not bind to either of the receptors.

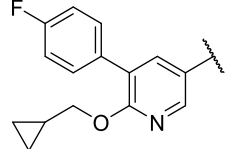
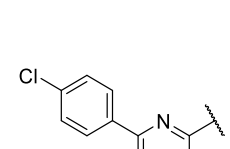
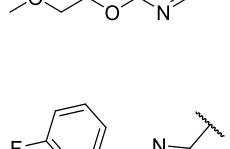
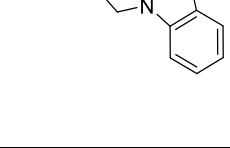
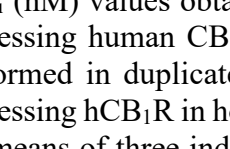
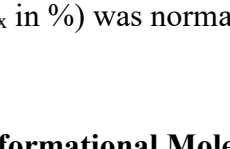
In summary, all NBD probes maintained CBR preference as observed with their corresponding DEG probe precursor structures in the linker screen (Table 2). In turn, installation of the sterically more demanding TAMRA dye was not tolerated well and led to a loss of CB₁R binding affinity except for probe **29**. This trend was further confirmed with two other small fluorophores of the “Scotfluor” series⁶⁰ (CB₁R-selective probes **51** and **52**, see Supporting Information Table S1). Our

investigation exemplifies again that careful pharmacological characterization is crucial for probe design.

Table 3. Binding affinities and functional activity of the fluorescent probes.



R ¹	Cmpd.	Dye	Binding affinity		Functional activity (cAMP assay)
			hCB ₁ R K _i (nM) ^a	hCB ₂ R K _i (nM) ^a	IC ₅₀ (nM) ^b (E _{max} (%)) ^c
	28	NBD	97	>10,000	16.6 (-62)
	29	TAMRA	2077	>10,000	102 (-64)
	30	NBD	428	>10,000	60.3 (-41)
	31	TAMRA	>10,000	>10,000	n.d.
	32	NBD	>10,000	309	n.d.
	33	TAMRA	>10,000	>10,000	n.d.

	40	NBD	>10,000	481	n.d.
	41	TAMRA	>10,000	>10,000	n.d.
	34	NBD	>10,000	701	n.d.
	35	TAMRA	>10,000	>10,000	n.d.
	36	NBD	1174	79	n.d.
	37	TAMRA	>10,000	983	n.d.

^a K_i (nM) values obtained from [³H]CP55,940 displacement assays on CHO membranes stably expressing human CB₁R or human CB₂R. Values are means of three independent experiments performed in duplicate. ^bThe activity levels (IC₅₀) of **28-30** were measured using cells stably expressing hCB₁R in homogeneous time-resolved fluorescence (HTRF) cAMP assay. The data are the means of three independent experiments performed in technical replicates. ^cMaximum effect (E_{max} in %) was normalized to reference full agonist CP55,940. n.d. is not determined.

Conformational Molecular Dynamics Simulation

While the classical construction principle of fluorescently labeled probes features several physicochemical characteristics that might hamper cellular permeation, we still observed rather efficient permeation at low concentration of probe **29** in the confocal imaging experiment (vide infra). Specifically, **29** has a high molecular weight, an increased number of rotatable bonds, a high topological polar surface area (tPSA), and is equipped with 5/6-TAMRA, which equilibrates in an (open) zwitterionic or a (closed) spirolactone form (Table 4 and Figure 4A).⁶¹⁻⁶⁴ We therefore investigated the unexpected membrane permeability of **29** by molecular dynamics (MD) simulations. For that, we hypothesized that **29** would effectively reduce its critically high PSA of >140 Å² by formation of intramolecular hydrogen bonds (IMHB) when entering an apolar

environment ('chameleonic effect').⁶⁵⁻⁶⁷ During a 50 ns MD simulation we analyzed the conformations of **29**, their 3D PSA, and the amount of formed IMHBs in water and *n*-octane (as a model of apolar cell membrane environment).

Probe **29** adopted a broad range of conformations with variable 3D PSA (see Figure 4B and Supporting Information Figure S13-19). Consistently the transition of compound **29** from water to *n*-octane would lead to a significant reduction of the mean 3D PSA and an increased number of IMHBs interactions, with the only exception being the spirolactone 6-isomer. For instance, the mean 3D PSA of the 5-zwitterion isomer (prevalent in water) would be reduced from 171.7 Å² to 99.8 Å² when transitioning into *n*-octane and equilibrating into the spirolactone form (prevalent in apolar solvents). Simultaneously the mean number IMHB of 0.1 in water would increase to 2.2 in *n*-octane (for other values see Supporting Information Table S4).

These MD data suggest that in particular the 5-isomer of **29** has a strong tendency for chameleonic effects. In addition, based on the 3D PSA, a better membrane permeability of probe **29** can be concluded than predicted by classical metrics of drug-likeness.⁶⁸ This shows that MD-derived studies for assessment of intracellular accessibility of high molecular weight compounds are relevant and useful also for fluorescent probe conjugates.^{65, 69}

Table 4: Calculated physicochemical descriptors of parent ligand **14** and probe **29** isomers as spirolactone and zwitterion forms by chemoinformatic tools.

Compd.	MW (g/mol) ^a	HBA ^a	HBD ^a	Rotatable bonds ^a	tPSA (Å ²) ^a
14	562.54	10	1	13	69.56
5/6- 29 spirolactone	1077.12	15	3	25	161.93

5/6-**29**
zwitterion

1077.12

15

3

26

179.44

⁶⁸“SwissADME.ch prediction by Swiss Institute of Bioinformatics.”

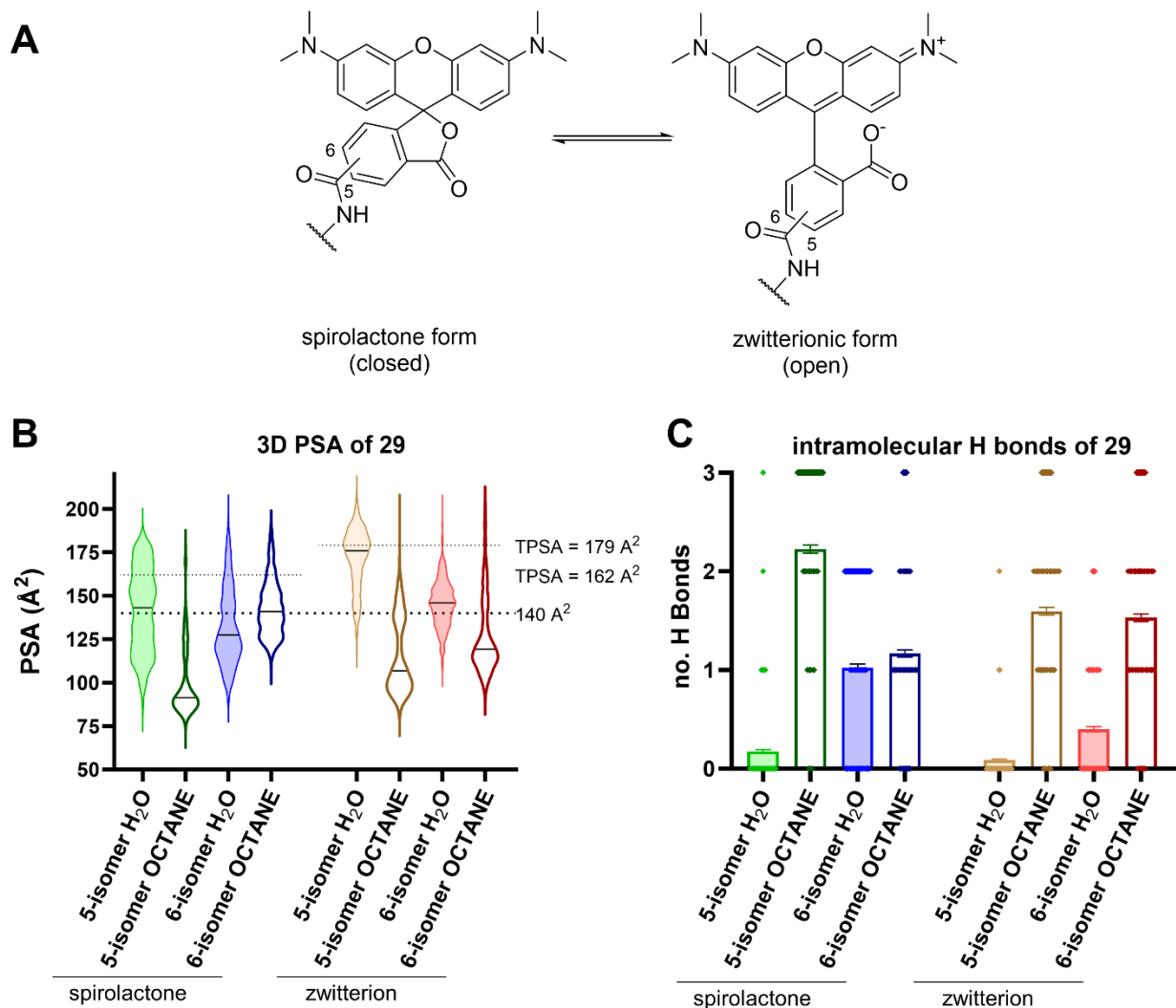


Figure 4: Conformational analysis of **29**. A) Equilibrium of 5/6-TAMRA isomers as spirolactone (closed) and zwitterionic (open) form. B) Violin plot of the 3D PSA distribution of the four possible isomers (open/closed, 5/6-isomer) of **29** in water and octane obtained by MD simulation (50 ns). Drug-like PSA cut-off 140 \AA^2 and tPSA of spirolactone and zwitterion form are indicated as dotted lines. Mean 3D PSA of each isomer is indicated as black line in the violin plot. C)

Intramolecular hydrogen bond formation observed in MD simulation (50 ns) of the four possible isomers (open/closed, 5/6-isomer) of **29** in water and octane. Mean hydrogen bond interactions represented as bar chart \pm SEM.

TR-FRET Binding Assay

TR-FRET has evolved as an attractive alternative to radioligand binding assays using fluorescent probes as tracers. TR-FRET assays are available for CB₁R⁷⁰⁻⁷² and especially suited for the determination of kinetic ligand-receptor interactions.^{73, 74} Consequently human embryonic kidney (HEK293TR) cells overexpressing SNAP-tagged hCB₁R were labeled with a SNAP-Lumi4-Tb FRET-donor and cell membranes prepared. Laser excitation of the terbium cryptate (337 nm) on the *N*-terminus of CB₁R induces energy transfer to a fluorescent probe when bound to CB₁R.

We first examined saturation and kinetic binding parameters of TAMRA probe **29** on CB₁R membrane preparations. The probe showed stable binding to the receptor over a time course of 30 min (Figure 5A). The saturation binding affinity value of **29** was lower ($K_D = 335.5$ nM) (Figure 5B) than obtained in the radioligand binding assay, yet, still in a commensurate range. In a kinetic association and dissociation experiment **29** exhibited a moderate association rate of 0.81×10^6 M⁻¹min⁻¹ on hCB₁R which supports its applicability as imaging probe (Table 5).

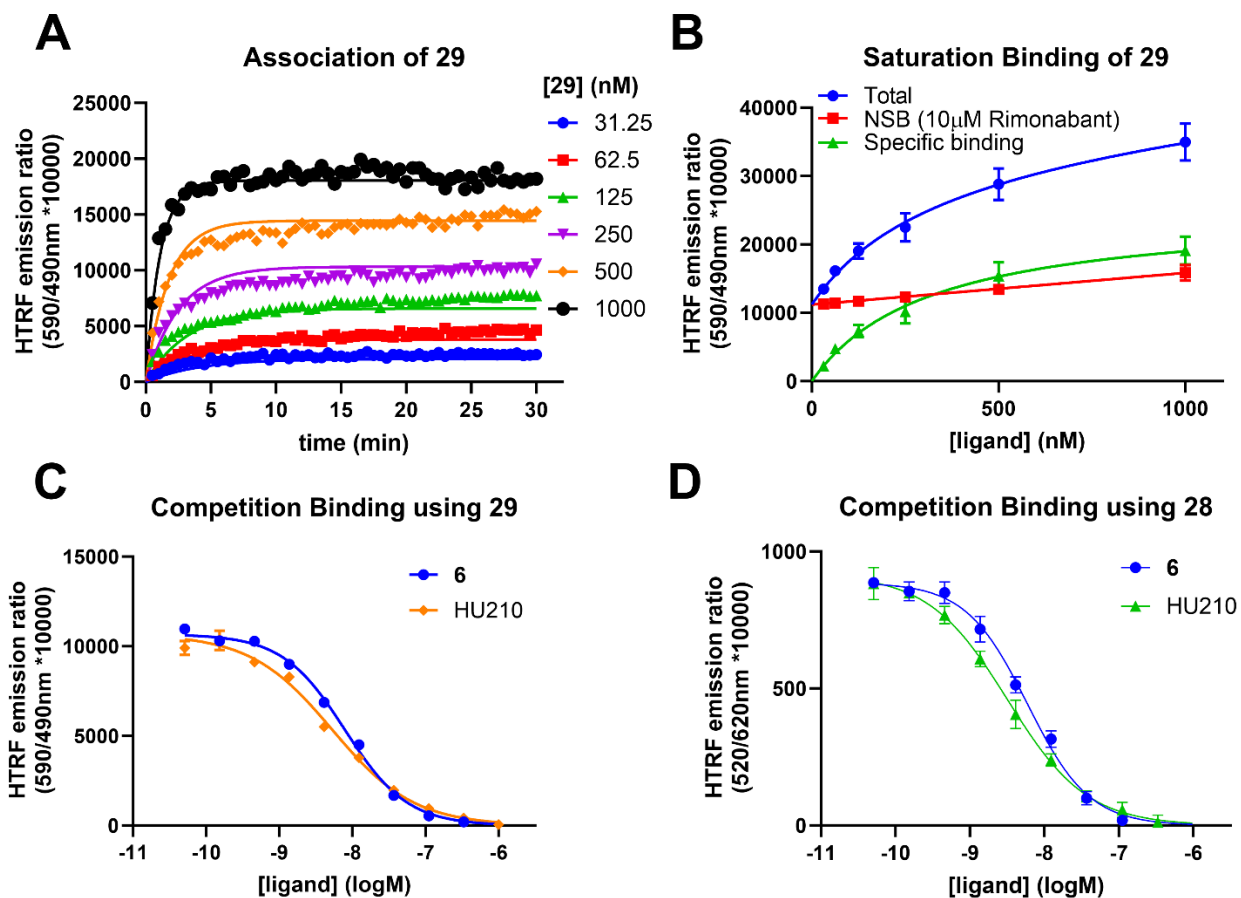


Figure 5. TR-FRET binding assays using HEK293TR-hCB₁R cell membranes. A) Observed association curves of TAMRA probe **29** to hCB₁R. B) Saturation binding analysis of **29** to hCB₁R after 60 min. C) Competition binding using **29** (300 nM) as tracer with increasing concentrations of CB₁R ligand **6** and HU210. D) Competition binding using NBD probe **28** (60 nM) as tracer with increasing concentrations of CB₁R ligand **6** and HU210. Kinetic and equilibrium data were fitted to the equations described in the Supporting Information to calculate K_D , k_{on} , and k_{off} values for fluorescent and unlabeled ligands. Data is presented as mean \pm SEM, $N = 3$.

Exploring the binding kinetics of a ligand is a crucial aspect of GPCR drug development and can be used to promote improved drug efficacy.⁷⁵ Using **29** as a fluorescent tracer the kinetic parameters k_{on} and k_{off} and resulting K_D of **6** and HU210 were determined (Table 5). In addition,

their equilibrium binding affinity was determined with both fluorescent NBD tracer **28** and TAMRA tracer **29** in a simple competition binding assay (Figure 5C+D, Table 5). Competition binding affinities K_i of the known CB₁R ligands were in excellent agreement with the kinetic K_D and literature radioligand binding affinities determined at human CB₁R.⁷⁶⁻⁷⁹ In addition, the determined K_i values of **6** and HU210 were probe independent. These experiments underscore the applicability of our fluorescent pyrazole probes **28** and **29** as highly useful tools in TR-FRET-based CB₁R drug discovery to characterize the kinetic binding and equilibrium affinities of CB₁R ligands in a potential high throughput setting avoiding radioactively labeled ligands.

Table 5: HTRF binding parameters of CB₁R probe **29** and unlabeled ligands^a

Compd.	k_{on} (10 ⁶ M ⁻¹ min ⁻¹)	k_{off} (min ⁻¹)	RT (min)	Kinetic K_D (nM)	K_i (nM) ^b	K_i (nM) ^c
29	0.81	0.26	3.85	365	-	-
6	48.3 ^b	0.15 ^b	6.67	3.23	3.34	2.08
HU210	37.4 ^b	0.11 ^b	9.10	3.04	2.08	1.26

^aData are presented as mean, $N = 3$. ^bProbe **29** (300 nM) used as tracer. ^cProbe **28** (60 nM) used as tracer. RT: residence time.

Fluorescence Confocal Microscopy in Live Cells

Having validated **29** as a selective and useful fluorescent probe for CB₁R pharmacology investigations we next examined its potential for visualization of human CB₁R on live SNAP-CB₁R-HEK293TR cells by confocal microscopy (Figure 6). For rigorous validation of selectivity and specificity, the experiments were performed side-by-side on tetracycline-inducible HEK293TR cells expressing CB₁R and CB₂R in comparison with parental HEK293TR cells without CBR expression. Probe **29** (λ_{Abs} : 555 nm, λ_{Em} : 585 nm, $\Phi = 37\%$ in PBS) was able to

selectively stain and visualize CB₁R on the HEK cells (Figure 6A) within 10 min (see also Supporting Information Video S1). In addition to membrane CB₁R, we observed intracellular staining of HEK293TR cells (Figure 6A, white arrow). Since **29** was shown to be an inverse agonist the possibility of ligand-induced internalization of membrane CB₁R by **29** was excluded.⁸⁰ Accordingly, probe **29** was able to passively permeate the outer cell membrane although exceeding typical drug-like parameters (see Table 4). This confirms the chameleonic behavior predicted by our MD simulation of probe **29**. In contrast, no staining was observed on CB₂R-HEK293TR or uninduced CB₁R-HEK293TR (Figure 6B and C). Similarly, the uninduced CB₂R-HEK293TR and HEK293TR cells without CBRs neither showed any staining nor unspecific background signal (Supporting Information Figure S3 and S4). The rapid staining (see Supporting Information Figure S5 and S6) and excellent CB₁R-selectivity and specificity emphasize the real-time imaging capabilities of probe **29** and correlate with the selectivity determined in the radioligand binding assay.

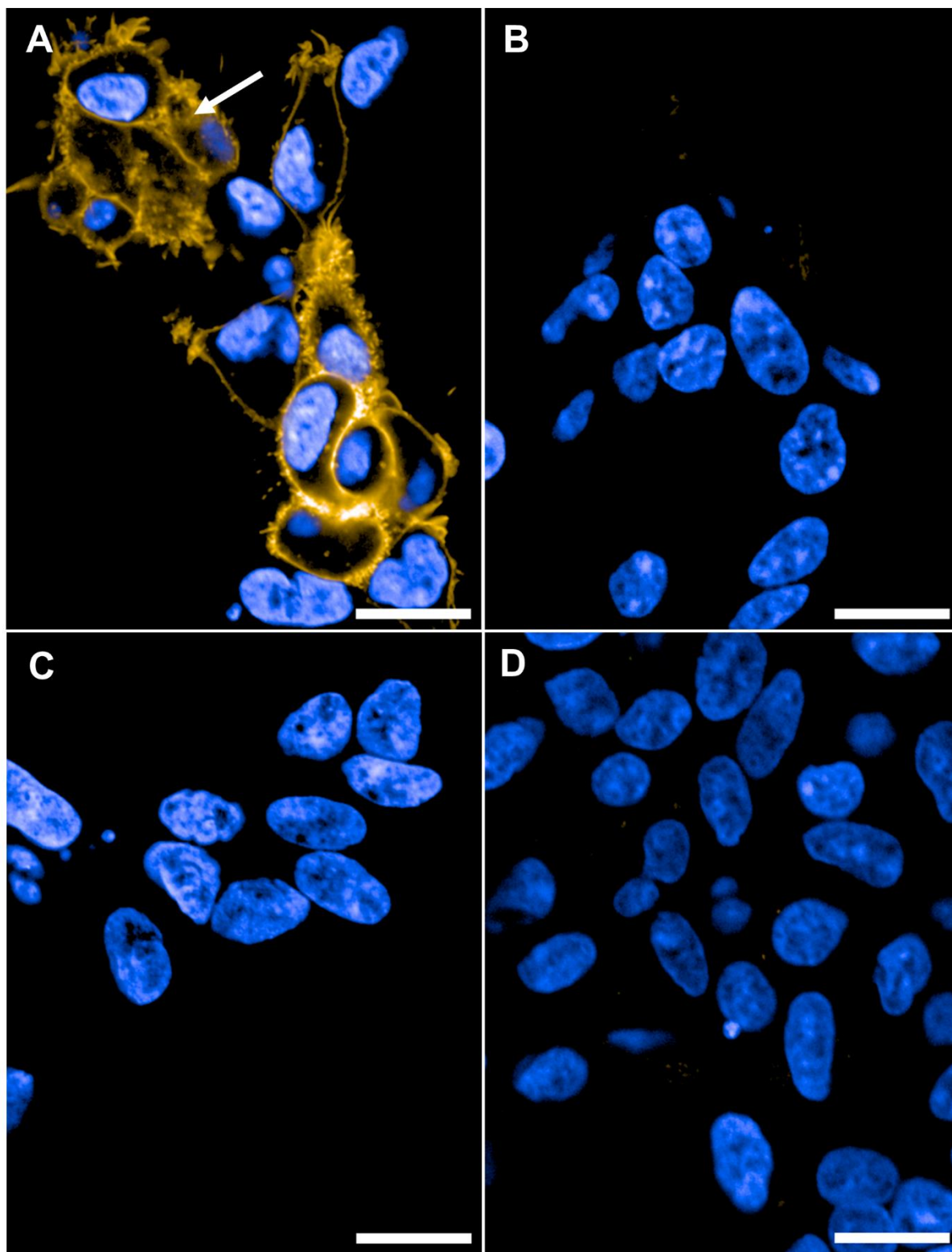


Figure 6. Live cell confocal imaging of HEK293TR cells. A) Induced CB₁R-HEK293TR cells incubated with **29** (250 nM, yellow). White arrow: Intracellular staining by **29**. B) Induced CB₂R-

HEK293TR cells incubated with **29** (250 nM, yellow). C) Uninduced CB₁R-HEK293TR cells incubated with **29** (250 nM, yellow). D) Induced CB₁R-HEK293TR cells incubated with **29** (250 nM, yellow) and competitor **6** (5 μM). Images recorded after 10 min at 63x magnification with nucleus counter stain Hoechst 33342 (blue). Scale bars 20 μm Images are representative of two to three independent experiments.

CONCLUSION

In summary, by using drug-like CB₁R ligands **5-10** we systematically explored the compatibility of our modular DEG-based CBR probe design approach. The screening from novel DEG ethyl esters **14-19** over PEG-linked compounds **22-27** to fluorescent probes **28-37** and **40-41** was guided by thorough pharmacological characterization and computational docking studies.

Our study showed that the DEG centerpiece can be used in combination with CB₁R pharmacophoric units. Unfortunately, while CB₁R binding and functional activity of the DEG ethyl esters was maintained, selectivity towards CB₁R was strongly compromised for most structures. Upon the linker exploration, this trend was solidified except for diarylpyrazole series **23a-d**, which turned into selective CB₁R binders. Optimal linker length and attachment site were investigated by docking studies and confirmed by SAR studies using radioligand displacement assays. Among the tested dyes NBD was well tolerated without affecting the probes selectivity profile. In contrast, TAMRA installation had detrimental effects on the CBR binding affinities, except for **29** and **37**. Most notably, throughout the exploration steps and among the tested structures pyrrole-based compounds (**14**, **22a-c**, **28**, **29**) exhibited outstanding selectivity towards CB₁R and tolerance for any modification. We characterized **28** and **29** as CB₁R-selective inverse agonist fluorescent probes with applicability in TR-FRET kinetic and equilibrium CB₁R ligand-

receptor binding studies. In live cell confocal fluorescence microscopy drug-derived **29** showed rapid, highly selective, and specific staining of CB₁R on HEK293TR cells. The observed membrane permeability of **29** was rationalized by *in silico* studies suggesting chameleonic effects.

Our novel building block strategy for probe design following reverse-design principles allowed the accomplishment of well-validated, selective, and specific tools for fluorescence-based CB₁R pharmacology. We believe that our CB₁R probes will pave the way for a deeper and broader understanding of CB₁R pharmacology in cannabinoid research.

REFERENCES

- (1) Battista, N.; Di Tommaso, M.; Bari, M.; Maccarrone, M. The endocannabinoid system: an overview. *Frontiers in Behavioral Neuroscience* **2012**, *6*. DOI: 10.3389/fnbeh.2012.00009.
- (2) Zou, S.; Kumar, U. Cannabinoid Receptors and the Endocannabinoid System: Signaling and Function in the Central Nervous System. *Int J Mol Sci* **2018**, *19* (3). DOI: 10.3390/ijms19030833.
- (3) Chou, S.; Ranganath, T.; Fish, K. N.; Lewis, D. A.; Sweet, R. A. Cell type specific cannabinoid CB1 receptor distribution across the human and non-human primate cortex. *Scientific Reports* **2022**, *12* (1). DOI: 10.1038/s41598-022-13724-x.
- (4) Maccarrone, M.; Bab, R.; Biro, T.; Cabral, G. A.; Dey, S. K.; Di Marzo, V.; Konje, J. C.; Kunos, G.; Mechoulam, R.; Pacher, P.; et al. Endocannabinoid signaling at the periphery: 50 years after THC. *Trends in Pharmacological Sciences* **2015**, *36* (5), 277-296. DOI: 10.1016/j.tips.2015.02.008.
- (5) O'Sullivan, S. E.; Yates, A. S.; Porter, R. K. The Peripheral Cannabinoid Receptor Type 1 (CB1) as a Molecular Target for Modulating Body Weight in Man. *Molecules* **2021**, *26* (20). DOI: 10.3390/molecules26206178.
- (6) Di Marzo, V.; Goparaju, S. K.; Wang, L.; Liu, J.; Bátkai, S.; Járαι, Z.; Fezza, F.; Miura, G. I.; Palmiter, R. D.; Sugiura, T.; et al. Leptin-regulated endocannabinoids are involved in maintaining food intake. *Nature* **2001**, *410* (6830), 822-825. DOI: Doi 10.1038/35071088.
- (7) Benard, G.; Massa, F.; Puente, N.; Lourenco, J.; Bellocchio, L.; Soria-Gomez, E.; Matias, I.; Delamarre, A.; Metna-Laurent, M.; Cannich, A.; et al. Mitochondrial CB(1) receptors regulate neuronal energy metabolism. *Nat Neurosci* **2012**, *15* (4), 558-564. DOI: 10.1038/nn.3053.
- (8) Toyoda, H. CB1 cannabinoid receptor-mediated plasticity of GABAergic synapses in the mouse insular cortex. *Sci Rep* **2020**, *10* (1), 7187. DOI: 10.1038/s41598-020-64236-5.
- (9) Milligan, A. L.; Szabo-Pardi, T. A.; Burton, M. D. Cannabinoid Receptor Type 1 and Its Role as an Analgesic: An Opioid Alternative? *Journal of Dual Diagnosis* **2020**, *16* (1), 106-119. DOI: 10.1080/15504263.2019.1668100.
- (10) Di Marzo, V.; Bifulco, M.; De Petrocellis, L. The endocannabinoid system and its therapeutic exploitation. *Nat Rev Drug Discov* **2004**, *3* (9), 771-784. DOI: 10.1038/nrd1495.
- (11) Pacher, P.; Batkai, S.; Kunos, G. The endocannabinoid system as an emerging target of pharmacotherapy. *Pharmacological Reviews* **2006**, *58* (3), 389-462. DOI: 10.1124/pr.58.3.2.
- (12) Amato, G.; Khan, N. S.; Maitra, R. A patent update on cannabinoid receptor 1 antagonists (2015-2018). *Expert Opinion on Therapeutic Patents* **2019**, *29* (4), 261-269. DOI: 10.1080/13543776.2019.1597851.
- (13) Vemuri, V. K.; Makriyannis, A. Medicinal chemistry of cannabinoids. *Clin Pharmacol Ther* **2015**, *97* (6), 553-558. DOI: 10.1002/cpt.115.
- (14) European Medicines Agency: *Questions and answers on the recommendation to suspend the marketing authorisation of Acomplia (rimonabant)*. 23 October 2008. https://www.ema.europa.eu/en/documents/medicine-qa/questions-answers-recommendation-suspend-marketing-authorisation-acomplia-rimonabant_en.pdf (accessed 31.10.2023).
- (15) Christensen, R.; Kristensen, P. K.; Bartels, E. M.; Bliddal, H.; Astrup, A. Efficacy and safety of the weight-loss drug rimonabant: a meta-analysis of randomised trials. *Lancet* **2007**, *370* (9600), 1706-1713. DOI: 10.1016/S0140-6736(07)61721-8.
- (16) Cristino, L.; Imperatore, R.; Di Marzo, V. Techniques for the Cellular and Subcellular Localization of Endocannabinoid Receptors and Enzymes in the Mammalian Brain. *Methods Enzymol* **2017**, *593*, 61-98. DOI: 10.1016/bs.mie.2017.05.003.

- (17) Bilic, S.; Dagon, Y.; Gustafson, T.; Johnson, L.; Lawler, J.; Rudolph-Own, L.; Gaich, G.; Tucker, E. OR03-2 Phase 1, Randomized, Controlled Trial of GFB-024, a Once-Monthly CB1 Inverse Agonist, in Healthy Overweight and Obese Participants and in Participants with Type 2 Diabetes Mellitus. *Journal of the Endocrine Society* **2022**, *6* (Supplement_1), A348-A348. DOI: 10.1210/jendso/bvac150.723 (accessed 1/19/2024).
- (18) Crater, G. D.; Lalonde, K.; Ravenelle, F.; Harvey, M.; Despres, J. P. Effects of CB1R inverse agonist, INV-202, in patients with features of metabolic syndrome. A randomized, placebo-controlled, double-blind phase 1b study. *Diabetes Obes Metab* **2024**, *26* (2), 642-649. DOI: 10.1111/dom.15353.
- (19) Galaj, E.; Hempel, B.; Moore, A.; Klein, B.; Bi, G. H.; Gardner, E. L.; Seltzman, H. H.; Xi, Z. X. Therapeutic potential of PIMSR, a novel CB1 receptor neutral antagonist, for cocaine use disorder: evidence from preclinical research. *Transl Psychiatry* **2022**, *12* (1), 286. DOI: 10.1038/s41398-022-02059-w.
- (20) Cinar, R.; Iyer, M. R.; Kunos, G. The therapeutic potential of second and third generation CB(1)R antagonists. *Pharmacol Ther* **2020**, *208*, 107477. DOI: 10.1016/j.pharmthera.2020.107477.
- (21) Bosquez-Berger, T.; Szanda, G.; Straiker, A. Requiem for Rimonabant: Therapeutic Potential for Cannabinoid CB1 Receptor Antagonists after the Fall. *Drugs and Drug Candidates* **2023**, *2* (3), 689-707.
- (22) Zawatsky, C. N.; Park, J. K.; Abdalla, J.; Kunos, G.; Iyer, M. R.; Cinar, R. Peripheral Hybrid CB(1)R and iNOS Antagonist MRI-1867 Displays Anti-Fibrotic Efficacy in Bleomycin-Induced Skin Fibrosis. *Front Endocrinol (Lausanne)* **2021**, *12*, 744857. DOI: 10.3389/fendo.2021.744857.
- (23) Jacquot, L.; Pointeau, O.; Roger-Villeboeuf, C.; Passilly-Degrace, P.; Belkaid, R.; Regazzoni, I.; Leemput, J.; Buch, C.; Demizieux, L.; Verges, B.; et al. Therapeutic potential of a novel peripherally restricted CB1R inverse agonist on the progression of diabetic nephropathy. *Front Nephrol* **2023**, *3*, 1138416. DOI: 10.3389/fneph.2023.1138416.
- (24) Monte, A.; Gorbenko, A.; Heuberger, J.; Cundy, K. C.; Klumpers, L.; Groeneveld, G. J. 304 Randomized Controlled Trial of ANEB-001 as an Antidote for Acute Cannabinoid Intoxication in Healthy Adults. *Annals of Emergency Medicine* **2023**, *82* (4), S133. DOI: 10.1016/j.annemergmed.2023.08.329 (accessed 2024/02/12).
- (25) Busquets Garcia, A.; Soria-Gomez, E.; Bellocchio, L.; Marsicano, G. Cannabinoid receptor type-1: breaking the dogmas. *F1000Res* **2016**, *5*. DOI: 10.12688/f1000research.8245.1.
- (26) Stoddart, L. A.; Kilpatrick, L. E.; Briddon, S. J.; Hill, S. J. Probing the pharmacology of G protein-coupled receptors with fluorescent ligands. *Neuropharmacology* **2015**, *98*, 48-57. DOI: 10.1016/j.neuropharm.2015.04.033.
- (27) Soave, M.; Briddon, S. J.; Hill, S. J.; Stoddart, L. A. Fluorescent ligands: Bringing light to emerging GPCR paradigms. *Br. J. Pharmacol.* **2020**, *177* (5), 978-991. DOI: 10.1111/bph.14953.
- (28) Stoddart, L. A.; Vernall, A. J.; Denman, J. L.; Briddon, S. J.; Kellam, B.; Hill, S. J. Fragment screening at adenosine-A(3) receptors in living cells using a fluorescence-based binding assay. *Chem Biol* **2012**, *19* (9), 1105-1115. DOI: 10.1016/j.chembiol.2012.07.014.
- (29) Cooper, S. L.; Soave, M.; Jorg, M.; Scammells, P. J.; Woolard, J.; Hill, S. J. Probe dependence of allosteric enhancers on the binding affinity of adenosine A(1) -receptor agonists at rat and human A(1) -receptors measured using NanoBRET. *Br. J. Pharmacol.* **2019**, *176* (7), 864-878. DOI: 10.1111/bph.14575.

- (30) Bruno, A.; Lembo, F.; Novellino, E.; Stornaiuolo, M.; Marinelli, L. Beyond radio-displacement techniques for identification of CB1 ligands: the first application of a fluorescence-quenching assay. *Sci Rep* **2014**, *4*, 3757. DOI: 10.1038/srep03757.
- (31) Stoddart, L. A.; Vernall, A. J.; Briddon, S. J.; Kellam, B.; Hill, S. J. Direct visualisation of internalization of the adenosine A3 receptor and localization with arrestin3 using a fluorescent agonist. *Neuropharmacology* **2015**, *98*, 68-77. DOI: 10.1016/j.neuropharm.2015.04.013.
- (32) Hern, J. A.; Baig, A. H.; Mashanov, G. I.; Birdsall, B.; Corrie, J. E.; Lazareno, S.; Molloy, J. E.; Birdsall, N. J. Formation and dissociation of M1 muscarinic receptor dimers seen by total internal reflection fluorescence imaging of single molecules. *Proc Natl Acad Sci U S A* **2010**, *107* (6), 2693-2698. DOI: 10.1073/pnas.0907915107.
- (33) Cordeaux, Y.; Briddon, S. J.; Alexander, S. P.; Kellam, B.; Hill, S. J. Agonist-occupied A3 adenosine receptors exist within heterogeneous complexes in membrane microdomains of individual living cells. *FASEB J.* **2008**, *22* (3), 850-860. DOI: 10.1096/fj.07-8180com.
- (34) Hamilton, A. J.; Payne, A. D.; Mocerino, M.; Gunosewoyo, H. Imaging Cannabinoid Receptors: A Brief Collection of Covalent and Fluorescent Probes for CB1 and CB2 Receptors. *Australian Journal of Chemistry* **2021**, *74* (6), 416-432. DOI: 10.1071/Ch21007.
- (35) Amenta, A.; Caprioglio, D.; Minassi, A.; Panza, L.; Passarella, D.; Fasano, V.; Imperio, D. Recent advances in the development of CB1R selective probes. *Frontiers in Natural Products* **2023**, *2*, Review. DOI: 10.3389/fntpr.2023.1196321.
- (36) Prokop, S.; Abranyi-Balogh, P.; Barti, B.; Vamosi, M.; Zoldi, M.; Barna, L.; Urban, G. M.; Toth, A. D.; Dudok, B.; Egyed, A.; et al. PharmacOSTORM nanoscale pharmacology reveals cariprazine binding on Islands of Calleja granule cells. *Nature Communications* **2021**, *12* (1). DOI: 10.1038/s41467-021-26757-z.
- (37) Martin-Fontecha, M.; Angelina, A.; Ruckert, B.; Rueda-Zubiaurre, A.; Martin-Cruz, L.; van de Veen, W.; Akdis, M.; Ortega-Gutierrez, S.; Lopez-Rodriguez, M. L.; Akdis, C. A.; et al. A Fluorescent Probe to Unravel Functional Features of Cannabinoid Receptor CB(1) in Human Blood and Tonsil Immune System Cells. *Bioconjug Chem* **2018**, *29* (2), 382-389. DOI: 10.1021/acs.bioconjchem.7b00680.
- (38) Grant, P. S.; Kahlcke, N.; Govindpani, K.; Hunter, M.; MacDonald, C.; Brimble, M. A.; Glass, M.; Furkert, D. P. Divalent cannabinoid-1 receptor ligands: A linker attachment point survey of SR141716A for development of high-affinity CB1R molecular probes. *Bioorganic & Medicinal Chemistry Letters* **2019**, *29* (21). DOI: 10.1016/j.bmcl.2019.126644.
- (39) Daly, C. J.; Ross, R. A.; Whyte, J.; Henstridge, C. M.; Irving, A. J.; McGrath, J. C. Fluorescent ligand binding reveals heterogeneous distribution of adrenoceptors and 'cannabinoid-like' receptors in small arteries. *Br. J. Pharmacol.* **2010**, *159* (4), 787-796. DOI: 10.1111/j.1476-5381.2009.00608.x.
- (40) Coutts, A. A.; Anavi-Goffer, S.; Ross, R. A.; MacEwan, D. J.; Mackie, K.; Pertwee, R. G.; Irving, A. J. Agonist-induced internalization and trafficking of cannabinoid CB1 receptors in hippocampal neurons. *J. Neurosci.* **2001**, *21* (7), 2425-2433. DOI: 10.1523/JNEUROSCI.21-07-02425.2001.
- (41) Guberman, M.; Kosar, M.; Omran, A.; Carreira, E. M.; Nazaré, M.; Grether, U. Reverse-Design toward Optimized Labeled Chemical Probes – Examples from the Endocannabinoid System. *CHIMIA* **2022**, *76* (5), 425. DOI: 10.2533/chimia.2022.425 (accessed 2022/12/06).
- (42) Gazzì, T.; Brennecke, B.; Atz, K.; Korn, C.; Sykes, D.; Forn-Cuni, G.; Pfaff, P.; Sarott, R. C.; Westphal, M. V.; Mostinski, Y.; et al. Detection of cannabinoid receptor type 2 in native cells and

zebrafish with a highly potent, cell-permeable fluorescent probe. *Chemical Science* **2022**, *13* (19), 5539-5545, 10.1039/D1SC06659E. DOI: 10.1039/D1SC06659E.

(43) Rover, S.; Andjelkovic, M.; Benardeau, A.; Chaput, E.; Guba, W.; Hebeisen, P.; Mohr, S.; Nettekoven, M.; Obst, U.; Richter, W. F.; et al. 6-Alkoxy-5-aryl-3-pyridinecarboxamides, a new series of bioavailable cannabinoid receptor type 1 (CB1) antagonists including peripherally selective compounds. *J. Med. Chem.* **2013**, *56* (24), 9874-9896. DOI: 10.1021/jm4010708.

(44) Rinaldi-Carmona, M.; Barth, F.; Heaulme, M.; Shire, D.; Calandra, B.; Congy, C.; Martinez, S.; Maruani, J.; Neliat, G.; Caput, D.; et al. SR141716A, a potent and selective antagonist of the brain cannabinoid receptor. *FEBS Lett.* **1994**, *350* (2-3), 240-244. DOI: 10.1016/0014-5793(94)00773-x.

(45) Mayweg, A.; Narquizian, R.; Pflieger, P.; Roever, S. PYRROLE OR IMIDAZOLE AMIDES FOR TREATING OBESITY. WO WO 2005/108393 A1, 2005.

(46) Hebeisen, P.; Iding, H.; Nettekoven Matthias, H.; Sander Ulrike, O.; Roever, S.; Weiss, U. R. S.; Wirz, B. Pyrazinecarboxamide derivatives as CB1 antagonists. US US 7629346 B2, 2009.

(47) Lazzari, P.; Distinto, R.; Manca, I.; Baillie, G.; Murineddu, G.; Pira, M.; Falzoi, M.; Sani, M.; Morales, P.; Ross, R.; et al. A critical review of both the synthesis approach and the receptor profile of the 8-chloro-1-(2',4'-dichlorophenyl)-N-piperidin-1-yl-1,4,5,6-tetrahydrobenzo[6,7]cyclohepta[1,2-c]pyrazole-3-carboxamide and analogue derivatives. *European Journal of Medicinal Chemistry* **2016**, *121*, 194-208. DOI: 10.1016/j.ejmech.2016.05.011.

(48) Schoeder, C. T.; Hess, C.; Madea, B.; Meiler, J.; Muller, C. E. Pharmacological evaluation of new constituents of "Spice": synthetic cannabinoids based on indole, indazole, benzimidazole and carbazole scaffolds. *Forensic Toxicology* **2018**, *36* (2), 385-403. DOI: 10.1007/s11419-018-0415-z.

(49) Katritzky, A. R.; Todadze, E.; Angrish, P.; Draghici, B. Efficient Peptide Coupling Involving Sterically Hindered Amino Acids. *The Journal of Organic Chemistry* **2007**, *72* (15), 5794-5801. DOI: 10.1021/jo0704255.

(50) Choy, J.; Jaime-Figueroa, S.; Jiang, L.; Wagner, P. Novel Practical Deprotection of N-Boc Compounds Using Fluorinated Alcohols. *Synthetic Communications* **2008**, *38* (21), 3840-3853. DOI: 10.1080/00397910802238718.

(51) Hua, T.; Vemuri, K.; Pu, M.; Qu, L.; Han, G. W.; Wu, Y.; Zhao, S.; Shui, W.; Li, S.; Korde, A.; et al. Crystal Structure of the Human Cannabinoid Receptor CB(1). *Cell* **2016**, *167* (3), 750-762 e714. DOI: 10.1016/j.cell.2016.10.004.

(52) Slavik, R.; Grether, U.; Herde, A. M.; Gobbi, L.; Fingerle, J.; Ullmer, C.; Krämer, S. D.; Schibli, R.; Mu, L. J.; Ametamey, S. M. Discovery of a High Affinity and Selective Pyridine Analog as a Potential Positron Emission Tomography Imaging Agent for Cannabinoid Type 2 Receptor. *J. Med. Chem.* **2015**, *58* (10), 4266-4277. DOI: 10.1021/acs.jmedchem.5b00283.

(53) Banister, S. D.; Moir, M.; Stuart, J.; Kevin, R. C.; Wood, K. E.; Longworth, M.; Wilkinson, S. M.; Beinat, C.; Buchanan, A. S.; Glass, M.; et al. Pharmacology of Indole and Indazole Synthetic Cannabinoid Designer Drugs AB-FUBINACA, ADB-FUBINACA, AB-PINACA, ADB-PINACA, 5F-AB-PINACA, 5F-ADB-PINACA, ADBICA, and 5F-ADBICA. *ACS Chem Neurosci* **2015**, *6* (9), 1546-1559. DOI: 10.1021/acschemneuro.5b00112.

(54) Degorce, F.; Card, A.; Soh, S.; Trinquet, E.; Knapik, G. P.; Xie, B. HTRF: A technology tailored for drug discovery - a review of theoretical aspects and recent applications. *Curr Chem Genomics* **2009**, *3*, 22-32. DOI: 10.2174/1875397300903010022.

- (55) Singh, S.; Oyagawa, C. R. M.; Macdonald, C.; Grimsey, N. L.; Glass, M.; Vernall, A. J. Chromenopyrazole-based High Affinity, Selective Fluorescent Ligands for Cannabinoid Type 2 Receptor. *Acs Medicinal Chemistry Letters* **2019**, *10* (2), 209-214. DOI: 10.1021/acsmchemlett.8b00597.
- (56) Cooper, A. G.; Oyagawa, C. R. M.; Manning, J. J.; Singh, S.; Hook, S.; Grimsey, N. L.; Glass, M.; Tyndall, J. D. A.; Vernall, A. J. Development of selective, fluorescent cannabinoid type 2 receptor ligands based on a 1,8-naphthyridin-2-(1)-one-3-carboxamide scaffold. *Medchemcomm* **2018**, *9* (12), 2055-2067. DOI: 10.1039/c8md00448j.
- (57) Spinelli, F.; Giampietro, R.; Stefanachi, A.; Riganti, C.; Kopecka, J.; Abatematteo, F. S.; Leonetti, F.; Colabufo, N. A.; Mangiatordi, G. F.; Nicolotti, O.; et al. Design and synthesis of fluorescent ligands for the detection of cannabinoid type 2 receptor (CB2R). *European Journal of Medicinal Chemistry* **2020**, *188*. DOI: 10.1016/j.ejmech.2020.112037.
- (58) Baker, J. G.; Middleton, R.; Adams, L.; May, L. T.; Briddon, S. J.; Kellam, B.; Hill, S. J. Influence of fluorophore and linker composition on the pharmacology of fluorescent adenosine A1 receptor ligands. *Br. J. Pharmacol.* **2010**, *159* (4), 772-786. DOI: 10.1111/j.1476-5381.2009.00488.x.
- (59) Yates, A. S.; Doughty, S. W.; Kendall, D. A.; Kellam, B. Chemical modification of the naphthoyl 3-position of JWH-015: in search of a fluorescent probe to the cannabinoid CB2 receptor. *Bioorg Med Chem Lett* **2005**, *15* (16), 3758-3762. DOI: 10.1016/j.bmcl.2005.05.049.
- (60) Benson, S.; Fernandez, A.; Barth, N. D.; de Moliner, F.; Horrocks, M. H.; Herrington, C. S.; Abad, J. L.; Delgado, A.; Kelly, L.; Chang, Z.; et al. SCOTfluors: Small, Conjugatable, Orthogonal, and Tunable Fluorophores for In Vivo Imaging of Cell Metabolism. *Angew. Chem. Int. Ed. Engl.* **2019**, *58* (21), 6911-6915. DOI: 10.1002/anie.201900465.
- (61) Lipinski, C. A.; Lombardo, F.; Dominy, B. W.; Feeney, P. J. Experimental and computational approaches to estimate solubility and permeability in drug discovery and development settings. *Adv Drug Deliv Rev* **2001**, *46* (1-3), 3-26. DOI: 10.1016/s0169-409x(00)00129-0.
- (62) Veber, D. F.; Johnson, S. R.; Cheng, H. Y.; Smith, B. R.; Ward, K. W.; Kopple, K. D. Molecular properties that influence the oral bioavailability of drug candidates. *J. Med. Chem.* **2002**, *45* (12), 2615-2623. DOI: 10.1021/jm020017n.
- (63) Wang, L.; Frei, M. S.; Salim, A.; Johnsson, K. Small-Molecule Fluorescent Probes for Live-Cell Super-Resolution Microscopy. *J Am Chem Soc* **2019**, *141* (7), 2770-2781. DOI: 10.1021/jacs.8b11134.
- (64) Wang, L.; Tran, M.; D'Este, E.; Roberti, J.; Koch, B.; Xue, L.; Johnsson, K. A general strategy to develop cell permeable and fluorogenic probes for multicolour nanoscopy. *Nat Chem* **2020**, *12* (2), 165-172. DOI: 10.1038/s41557-019-0371-1.
- (65) Matsson, P.; Doak, B. C.; Over, B.; Kihlberg, J. Cell permeability beyond the rule of 5. *Adv Drug Deliv Rev* **2016**, *101*, 42-61. DOI: 10.1016/j.addr.2016.03.013.
- (66) David, L.; Wenlock, M.; Barton, P.; Ritzen, A. Prediction of Chameleonic Efficiency. *ChemMedChem* **2021**, *16* (17), 2669-2685. DOI: 10.1002/cmdc.202100306.
- (67) Poongavanam, V.; Wieske, L. H. E.; Peintner, S.; Erdelyi, M.; Kihlberg, J. Molecular chameleons in drug discovery. *Nat Rev Chem* **2024**, *8* (1), 45-60. DOI: 10.1038/s41570-023-00563-1.
- (68) Daina, A.; Michielin, O.; Zoete, V. SwissADME: a free web tool to evaluate pharmacokinetics, drug-likeness and medicinal chemistry friendliness of small molecules. *Sci Rep* **2017**, *7*, 42717. DOI: 10.1038/srep42717.

- (69) Poongavanam, V.; Atilaw, Y.; Siegel, S.; Giese, A.; Lehmann, L.; Meibom, D.; Erdelyi, M.; Kihlberg, J. Linker-Dependent Folding Rationalizes PROTAC Cell Permeability. *J. Med. Chem.* **2022**, *65* (19), 13029-13040. DOI: 10.1021/acs.jmedchem.2c00877.
- (70) Sykes, D. A.; Borrega-Roman, L.; Harwood, C. R.; Hoare, B.; Lochray, J. M.; Gazzi, T.; Briddon, S. J.; Nazaré, M.; Grether, U.; Hill, S. J.; et al. Kinetic Profiling of Ligands and Fragments Binding to GPCRs by TR-FRET. In *Biophysical and Computational Tools in Drug Discovery*, Saxena, A. K. Ed.; Springer International Publishing, 2021; pp 1-32.
- (71) Navarro, G.; Sotelo, E.; Raich, I.; Loza, M. I.; Brea, J.; Majellaro, M. A Robust and Efficient FRET-Based Assay for Cannabinoid Receptor Ligands Discovery. *Molecules* **2023**, *28* (24). DOI: 10.3390/molecules28248107.
- (72) Raich, I.; Rivas-Santisteban, R.; Lillo, A.; Lillo, J.; Reyes-Resina, I.; Nadal, X.; Ferreira-Vera, C.; de Medina, V. S.; Majellaro, M.; Sotelo, E.; et al. Similarities and differences upon binding of naturally occurring Delta(9)-tetrahydrocannabinol-derivatives to cannabinoid CB(1) and CB(2) receptors. *Pharmacol. Res.* **2021**, *174*, 105970. DOI: 10.1016/j.phrs.2021.105970.
- (73) Schiele, F.; Ayaz, P.; Fernandez-Montalvan, A. A universal homogeneous assay for high-throughput determination of binding kinetics. *Anal. Biochem.* **2015**, *468*, 42-49. DOI: 10.1016/j.ab.2014.09.007.
- (74) Sykes, D. A.; Stoddart, L. A.; Kilpatrick, L. E.; Hill, S. J. Binding kinetics of ligands acting at GPCRs. *Molecular and Cellular Endocrinology* **2019**, *485*, 9-19. DOI: 10.1016/j.mce.2019.01.018.
- (75) Copeland, R. A.; Pompliano, D. L.; Meek, T. D. Drug-target residence time and its implications for lead optimization (vol 5, pg 730, 2006). *Nature Reviews Drug Discovery* **2007**, *6* (3), 249-249.
- (76) Muccioli, G. G.; Wouters, J.; Charlier, C.; Scriba, G. K.; Pizza, T.; Di Pace, P.; De Martino, P.; Poppitz, W.; Poupaert, J. H.; Lambert, D. M. Synthesis and activity of 1,3,5-triphenylimidazolidine-2,4-diones and 1,3,5-triphenyl-2-thioxoimidazolidin-4-ones: characterization of new CB1 cannabinoid receptor inverse agonists/antagonists. *J. Med. Chem.* **2006**, *49* (3), 872-882. DOI: 10.1021/jm050484f.
- (77) Manera, C.; Cascio, M. G.; Benetti, V.; Allara, M.; Tuccinardi, T.; Martinelli, A.; Saccomanni, G.; Vivoli, E.; Ghelardini, C.; Di Marzo, V.; et al. New 1,8-naphthyridine and quinoline derivatives as CB2 selective agonists. *Bioorganic & Medicinal Chemistry Letters* **2007**, *17* (23), 6505-6510. DOI: 10.1016/j.bmcl.2007.09.089.
- (78) Srivastava, B. K.; Johrapurkar, A.; Raval, S.; Patel, J. Z.; Soni, R.; Raval, P.; Gite, A.; Goswami, A.; Sadhwani, N.; Gandhi, N.; et al. Diaryl dihydropyrazole-3-carboxamides with significant in vivo antiobesity activity related to CB1 receptor antagonism: synthesis, biological evaluation, and molecular modeling in the homology model. *J. Med. Chem.* **2007**, *50* (24), 5951-5966. DOI: 10.1021/jm061490u.
- (79) Donohue, S. R.; Pike, V. W.; Finnema, S. J.; Truong, P.; Andersson, J.; Gulyás, B.; Halldin, C. Discovery and labeling of high-affinity 3,4-diarylpyrazolines as candidate radioligands for in vivo imaging of cannabinoid subtype-1 (CB1) receptors. *J. Med. Chem.* **2008**, *51* (18), 5608-5616. DOI: 10.1021/jm800329z.
- (80) Wu, D. F.; Yang, L. Q.; Goschke, A.; Stumm, R.; Brandenburg, L. O.; Liang, Y. J.; Holtt, V.; Koch, T. Role of receptor internalization in the agonist-induced desensitization of cannabinoid type 1 receptors. *J. Neurochem.* **2008**, *104* (4), 1132-1143. DOI: 10.1111/j.1471-4159.2007.05063.x.

- (81) Cheng, Y.; Prusoff, W. H. Relationship between Inhibition Constant (K₁) and Concentration of Inhibitor Which Causes 50 Per Cent Inhibition (I₅₀) of an Enzymatic-Reaction. *Biochem. Pharmacol.* **1973**, 22 (23), 3099-3108.
- (82) Fulmer, G. R.; Miller, A. J. M.; Sherden, N. H.; Gottlieb, H. E.; Nudelman, A.; Stoltz, B. M.; Bercaw, J. E.; Goldberg, K. I. NMR Chemical Shifts of Trace Impurities: Common Laboratory Solvents, Organics, and Gases in Deuterated Solvents Relevant to the Organometallic Chemist. *Organometallics* **2010**, 29 (9), 2176-2179. DOI: 10.1021/om100106e.
- (83) Murineddu, G.; Lazzari, P.; Ruiu, S.; Sanna, A.; Loriga, G.; Manca, I.; Falzoi, M.; Dessì, C.; Curzu, M. M.; Chelucci, G.; et al. Tricyclic pyrazoles.: 4.: Synthesis and biological evaluation of analogues of the robust and selective CB cannabinoid ligand 1-(2',4'-dichlorophenyl)-6-methylpiperidin-1-yl-1,4-dihydroindeno[1,2-c]pyrazole-3-carboxamide. *J. Med. Chem.* **2006**, 49 (25), 7502-7512. DOI: 10.1021/jm060920d.
- (84) Longworth, M.; Banister, S. D.; Boyd, R.; Kevin, R. C.; Connor, M.; McGregor, I. S.; Kassiou, M. Pharmacology of Cumyl-Carboxamide Synthetic Cannabinoid New Psychoactive Substances (NPS) CUMYL-BICA, CUMYL-PICA, CUMYL-5F-PICA, CUMYL-5F-PINACA, and Their Analogues. *Acs Chemical Neuroscience* **2017**, 8 (10), 2159-2167. DOI: 10.1021/acscchemneuro.7b00267.